Preparation and Characterization of Linear Low-Density Polyethylene/Dickite Nanocomposites Prepared by the Direct Melt Blending of Linear Low-Density Polyethylene with Exfoliated Dickite

Bing Xue,[1] Peiping Zhang,[1] Yinshan Jiang,[1] Mengmeng Sun,[1] Darui Liu,[1] Lixin Yu[2]

[1]*Key Laboratory of Automobile Materials of Ministry of Education and Department of Materials Science and Engineering, Jilin University, Changchun 130025, China*
[2]*School of Materials Science and Engineering, Department of Inorganic Nonmetal Materials Science, Nanchang University, Nanchang 330031, China*

Received 23 April 2010; accepted 29 August 2010
DOI 10.1002/app.33324
Published online 1 December 2010 in Wiley Online Library (wileyonlinelibrary.com).

ABSTRACT: Dickite particles were exfoliated by the thermal decomposition of molecular urea in the interlayer of dickite. The exfoliated dickite (ED) was composed with linear low-density polyethylene (LLDPE) to prepare a novel LLDPE/dickite nanocomposite (LDN-5). X-ray diffraction (XRD), Fourier transform infrared (FTIR) spectroscopy, scanning electron microscopy (SEM), and transmission electron microscopy (TEM) were used to evaluate the exfoliation effect. FTIR spectra showed that the inner-surface hydroxyls of dickite decreased because of the sufficient exfoliation of the dickite layers. The 001 diffraction of dickite in the XRD pattern almost disappeared after exfoliation; this indicated the random orientation of dickite platelets. SEM and TEM micrographs confirmed the effective thermal decomposition of the interlamellar molecular urea ED layers, which resulted in smaller particle sizes and better dispersions of dickite in the resulting LLDPE/dickite composite. The microstructure of LDN-5 showed that most of the dickite platelets were exfoliated and homogeneously dispersed in the LLDPE; this led to increases in the anticorrosion properties and thermal stabilities of LDN-5. The results of salt-spray tests illustrated that the corrosion rate of the iron coupon decreased from 23% (LLDPE packing) to 0.4% (LDN-5 packing). Moreover, the thermal degradation temperature corresponding to a mass loss of 10% increased from 330°C (pure LLDPE) to 379°C (LDN-5). © 2010 Wiley Periodicals, Inc. J Appl Polym Sci 120: 1736–1743, 2011

Key words: fillers; lamellar; nanocomposites

INTRODUCTION

Polyethylene (PE) is one of the most widely used polyolefins in the packaging industry because of its good flexibility, better water vapor barrier properties, considerable chemical resistance, and high transparency.[1] However, organic packaging is not impermeable, and widespread defects create many small pathways for corrosive species to reach packaged products, especially metal products, and localized corrosion occurs.[2] The corrosion of metal products become even worse under aggressive marine conditions. Although several efficient methods of corrosion protection, such as antirust oil sealing,[3] dryness packaging, and multilayer structures,[4,5] have been developed, most commercial applications designed as a combination of vapor-phase corrosion inhibitor (VCI)[6,7] and PE. VCI effectively inhibits the corrosion of metals, but more environmentally friendly products are demanded because VCI is harmful to the human body and our environment.

The addition of clays into a polymer matrix is thought to result in a remarkable improvement of barrier properties, mainly because of a tortuosity-driven decrease in the molecular diffusion of gases and vapors.[8] Furthermore, it has been broadly reported in the literature that the addition of nanoclays into a pure polymer to form polymer/clay nanocomposites increases some relevant material properties, such as mechanical resistance,[9,10] thermal stability,[11] and electrical conductivity, without significant reductions in the toughness and transparency.[12,13] Among the nanocomposites, the most widely used clay is montmorillonite.[14–16] It has been pointed out that the properties of polymer/clay nanocomposites also depend on the kind of clay used.[9] This prompts us to survey

Correspondence to: P. Zhang (peiping_zhang@yahoo.com.cn).
Contract grant sponsor: National Natural Science Foundation of China; contract grant numbers: 50574043 and 40772028.
Contract grant sponsor: Project 985-Automotive Engineering of Jilin University.

the possibility of the formation of novel nanocomposites with different kinds of clays.

Dickite [$Al_2Si_2O_5(OH)_4$], a 1 : 1 type clay mineral, is different from 2 : 1 type smectite clay minerals. The surface of the aluminosilicate is composed of SiO_4 tetrahedral sheets and $AlO_2(OH)_4$ octahedral sheets[17] which can be used for the formation of hydrogen bonding with some polymers.[9] Because of its unique structural features, polymer/dickite nanocomposites would exhibit different behaviors from those of polymer/smectite nanocomposites. Our previous studies[18] have found that even large dickite particles simply modified by common modifying agents effectively improve the salt-spray barrier properties of linear low-density polyethylene (LLDPE). Thus, if dickite particles could be dispersed in the nanoscale, the anticorrosion properties of LLDPE/dickite composites may be further improved. However, reports on polymer/dickite nanocomposites are very rare.

In this study, we used the thermal decomposition of interlamellar molecular urea as a novel method to exfoliate dickite platelets into the nanoscale. Molecular urea was first introduced into the interlayer space of dickite. After calcination, the dickite was efficiently exfoliated and melt-compounded with LLDPE to prepare a novel LLDPE/dickite nanocomposite (LDN-5). The anticorrosion properties of the resulting material were examined by salt-spray tests to determine if it met the requirements for maritime packaging applications. The morphological characteristics and thermal properties of the material developed were also examined as a function of the composition.

EXPERIMENTAL

Chemical

An 80% hydrazine monohydrate solution was obtained from BASF Chemical (Tianjin, China) Co., Ltd. Urea and stearic acid were analytically pure reagents and were purchased from Shanghai Chemical Regents (Shanghai, China) Co. LLDPE was provided from Jilin Petrochemical (Jilin, China) Co., Ltd. The compatibilizer {maleic anhydride grafted LLDPE and tetra[methylene-β-(3,5-di-*tert*-butyl-4-hydroxyphenyl)-propionate] methane (antioxidant-LH)} were obtained from Nanjing Deba Chemical (Nanjing, China) Co., Ltd. All chemicals are used as received without further purification. The dickite powder came from Chang-Bai (Baishan, Jilin Province, China). This specimen was quite pure, and little impurity was detected.

Preparation of the dickite–urea intercalation complex

The dickite–urea intercalation complex was prepared as a precursor for the exfoliation of dickite via a two-step process. First, 3 g of dickite powder and 20 mL of an 80% hydrazine monohydrate solution were placed in a 50-mL vessel and stirred with a magnetic stirrer at 25°C for 24 h. The product was filtered and dried *in vacuo* at 50°C and crushed in a mortar, and the dickite–hydrazine intercalation complex was obtained. Then, 20 mL of a 10 mol/L urea solution and 3 g of the dickite–hydrazine intercalation complex were added to a 50-mL vessel and stirred with a magnetic stirrer at 25°C for 1 h. The excess solution was removed by centrifugation. After that, another 20 mL of a 10 mol/L urea solution was added to the 50-mL vessel, and we repeated the previous process. The product was dried *in vacuo* at 50°C and crushed in a mortar. The dickite–urea intercalation complex was obtained.

Preparation of the exfoliated dickite (ED)

We obtained ED by rapidly putting the dickite–urea intercalation complex into a 500°C Muffle furnace. A 3-min reaction caused complete thermal decomposition of the molecular urea, and ED was obtained.

Preparation of LDN-5

LDN-5 was prepared via a two-step melt compounding process. First, ED, the compatibilizer, antioxidant-LH, and LLDPE were mixed in a SLJ-40 internal mixer (Education Apparatus Co., Changchun, China) at 170°C for 30 min at a speed of 50 rpm. The total quantity of ED, LLDPE, compatibilizer, and antioxidant-LH added to the internal mixer was 40 g. Second, the sample removed from the internal mixer was extruded with a single-screw extruder (Education Apparatus) at 170°C at a screw speed of 50 rpm. Before melt compounding with LLPDE, ED was modified by stearic acid under experimental conditions described previously[18] to improve the compatibility between the clay and nonpolar LLDPE matrix. For comparison, original dickite (OD) was used to prepare the LLDPE/dickite microcomposite (LDM-5) under the same conditions. Also, pure LLDPE was treated with the same compounding process. The compositions of the prepared composites are listed in Table I.

Characterization

The X-ray diffraction (XRD) study of LLDPE/dickite composites was performed on an X'Pert PRO diffractometer (Almelo, The Netherlands) with Cu Kα radiation (1.5418 Å) at 50 kV and 250 mA.

Fourier transform infrared (FTIR) spectroscopy of the samples was carried out on a Nexus 670 auto FTIR spectrometer (Madison, Wisconsin, U.S.), for which samples were pelletized with KBr powder.

TABLE I
Compositions of the Prepared Composites

Sample	Filler (wt %)	Compatibilizer (wt %)	Antioxidant (wt %)	LLDPE (wt %)
LLDPE	—	—	—	100
LDN-5	5 (ED)	5	1	89
LDM-5	5 (OD)	5	1	89

Microscopic observations of the dickite and LDN-5 were performed in a Quanta200 environmental scanning electron microscope (Hillsboro, Oregon, U.S.) and a JEOL JEM-1011 transmission electron microscope (Tokyo, Japan).

The salt-spray test, which could simulate an ocean environment, was performed in a YW/R-150 salt-mist corrosion testing box (Tianjin Surui Co., Ltd., Tianjin, China), according to ASTM B-117 (natural salt-spray test) with the following conditions: the NaCl concentration of the sprayed solution was 50 g/L (5%NaCl), the pH was between 6.5 and 7.2, and the temperature remained at 35°C. The prepared composites and LLDPE were pressed into a thin film with a thickness of about 0.1 mm in an X-20 heat former machine (Education Apparatus). The film was made into small bags with a size of 40 × 40 mm^2. Then, clean round iron (Q195 steel) coupons were sealed in the prepared bags. These bags were hung inside the testing box with plastic strings in free-standing mode to ensure that both sides of the bags got sprayed uniformly. For comparison, a Daubert Cromwell VCI film (Chicago, Illinois, U.S.) was also tested by the salt-spray test.

Thermogravimetry (TG) testing was carried on a WCT-2C thermoanalyzer (Optics Apparatus Co., Beijing, China). The samples were heated from ambient laboratory temperature (ca. 25°C) to 700°C at a rate of 15°C/min under a natural air atmosphere and with Al_2O_3 as the inert reference.

RESULTS AND DISCUSSION

XRD analysis

The XRD patterns of dickite and the LLDPE/dickite composites are given in Figure 1. Figure 1(b) displays the 001 diffraction at 7.22 Å of OD. As shown in Figure 1(c), the basal 001 diffraction of dickite disappeared, and a new peak appeared with a *d* value of 10.68 Å; this indicated the intercalation of urea into the dickite interlayer and the complete expansion of the dickite structure from a basal spacing of 7.22 Å to one of 10.68 Å. The peak broadening and intensity reduction in the 2θ region between 20 and 23° was attributed to elastic deformation of the layers[19] and partial amorphization of the dickite phase during the intercalation process.[20] On the other hand, the characteristic peaks of urea at 3.99, 3.62, 3.05, and 2.82 Å were observed in the XRD pattern of the dickite–urea intercalation complex; this confirmed the existence of the reagent. As shown in Figure 1(d), the 001 diffraction of dickite almost disappeared; this indicated the random orientation of the dickite platelets. This situation was attributed to the fact that the temperature of 500°C in the Muffle furnace was enough to rapidly decompose the urea molecules in the interlayer of the dickite–urea intercalation complex. Urea and absorbed water may have undergone the following reaction:[21]

$$NH_2—CO—NH_2 + H_2O \rightarrow 2NH_3 + CO_2 \quad (1)$$

Meanwhile, urea may have undergone other reactions:[22]

$$NH_2—CO—NH_2 \rightarrow H—O—C \equiv N + NH_3 \quad (2)$$

$$3NH_2—CO—NH_2 \rightarrow (H—O)_3C_3N_3 + 3NH_3 \quad (3)$$

The large amount of gases generated from the decomposition of urea expanded the dickite interlayer and led to the exfoliation of the dickite layers.

When ED composed with LLDPE, the 001 diffraction of dickite remained unchanged; this indicated that the ED platelets were well dispersed in the LLDPE matrix [Fig. 1(g)]. The surface hydrophobic modification of dickite and the process of melt mixing combined with melt extruding played an important role in dispersing the ED platelets in LLDPE and preventing the agglomeration of dickite platelets. Meanwhile, the residual 001 diffraction of dickite shown in Figure 1(g) suggested that part of the dickite particles was not exfoliated. However, a great

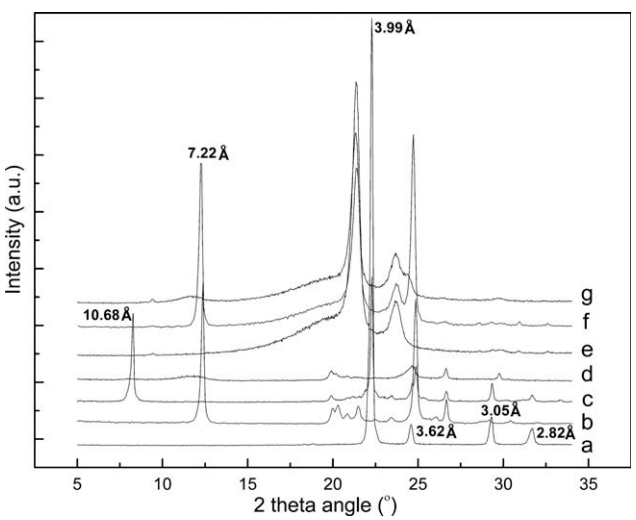

Figure 1 XRD patterns of (a) urea, (b) OD, (c) dickite–urea intercalation complex, (d) ED, (e) LLDPE, (f) LDM-5, and (g) LDN-5.

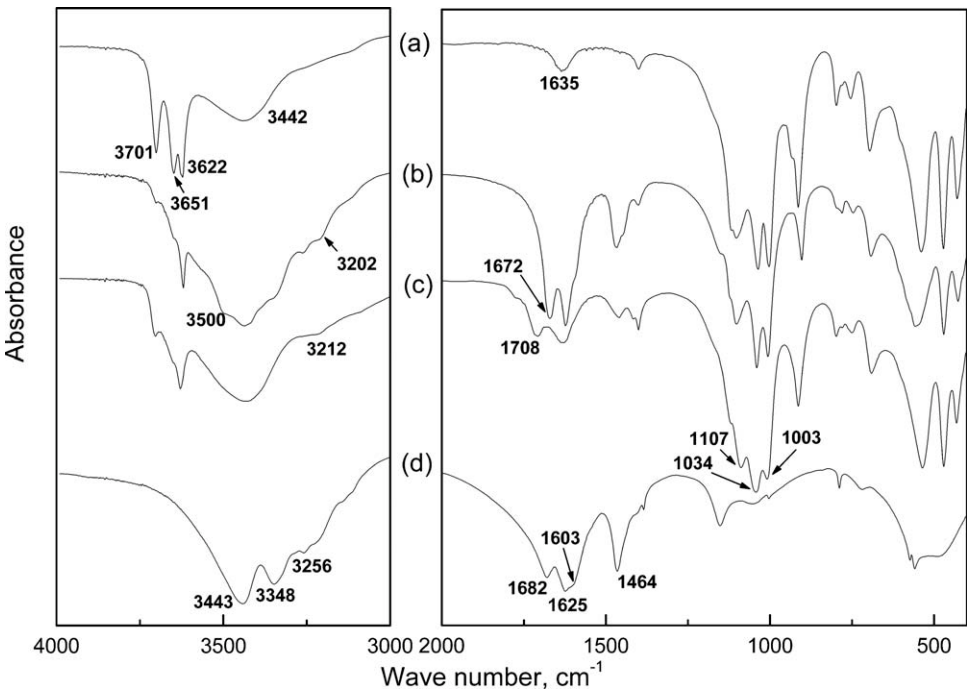

Figure 2 FTIR spectra of (a) OD, (b) dickite–urea intercalation complex, (c) ED, and (d) urea.

proportion of the clay remained exfoliated in the nanocomposite.

FTIR spectral analysis

The FTIR spectra of OD, the dickite–urea intercalation complex, and ED are shown in Figure 2. As shown in Figure 2(a), the spectrum of OD exhibited Si—O stretching bands at 1003, 1034 and 1107 cm^{-1}, which together with OH stretching vibration at 3622, 3651, and 3701 cm^{-1}, were characteristic for dickite. The absorption band at 3622 was attributed to inner hydroxyl groups, lying between the tetrahedral and the octahedral sheets. The other two OH groups resided at the octahedral surface of the silicate layers and formed weak hydrogen bonds with the oxygens of the Si—O—Si bonds on the lower surface of the next layer.[23] The additional broad stretching bands of dickite at 3442 and 1635 cm^{-1} were attributed to associated water adsorbed on the external surface. The FTIR spectra of urea had bands at 3256, 3348, and 3443 cm^{-1} (symmetric and asymmetric stretching vibrations of the N—H); 1603, 1625, and 1682 cm^{-1} (assigned to C=O vibrations), and 1464 cm^{-1} (C—N stretching vibration).[20]

Compared with OD, as clearly shown in Figure 2(b), the 3622-cm^{-1} vibration band remained the same, but the intensity of the 3701-cm^{-1} peak decreased, and the 3651-cm^{-1} peak almost disappeared. These results show that the OH groups of the interlayer surface were disturbed because of the intercalation of molecular urea into the dickite interlayer space. The new bands at 3202 and 3500 cm^{-1} were attributed to the formation of hydrogen bonds between the NH_2 groups of urea and the oxygens of the basal tetrahedral sheet.[20,24,25] The formation of hydrogen bonds with hydroxyl groups shifted the stretching frequency of urea from 1682 to 1672 cm^{-1}, as shown in Figure 2(b). This situation may have been due to molecular urea lingering between the dickite layers. When we analyzed the FTIR spectra of the dickite–urea intercalation complex, we also found that there were characteristic absorption peaks of urea at 1464, 1625, 3256, 3348, and 3443 cm^{-1}.

The FTIR spectra of ED showed similar vibrations of the inner and inner-surface hydroxyls to the dickite–urea intercalation complex. Compared with the dickite–urea intercalation complex, the intensity of the 3651 and 3701-cm^{-1} peak increased slightly, as shown in Figure 2(c); this indicated the enhanced interaction of OH groups in the interlayer surface. The temperature of 500°C in the Muffle furnace was hot enough to rapidly decompose the urea molecules in the interlayer of the dickite–urea intercalation complex. A small part of the dickite platelets tried to restore the original arrangement along basal planes, and therefore, a slightly enhanced interaction of the OH groups of the interlayer surface was observed in the FTIR spectra. However, the vibration intensity of the inner-surface hydroxyls of ED could not compare with that of OD. The evidence showed that most of the dickite particles were exfoliated. In addition, ED had additional bands. The bands at

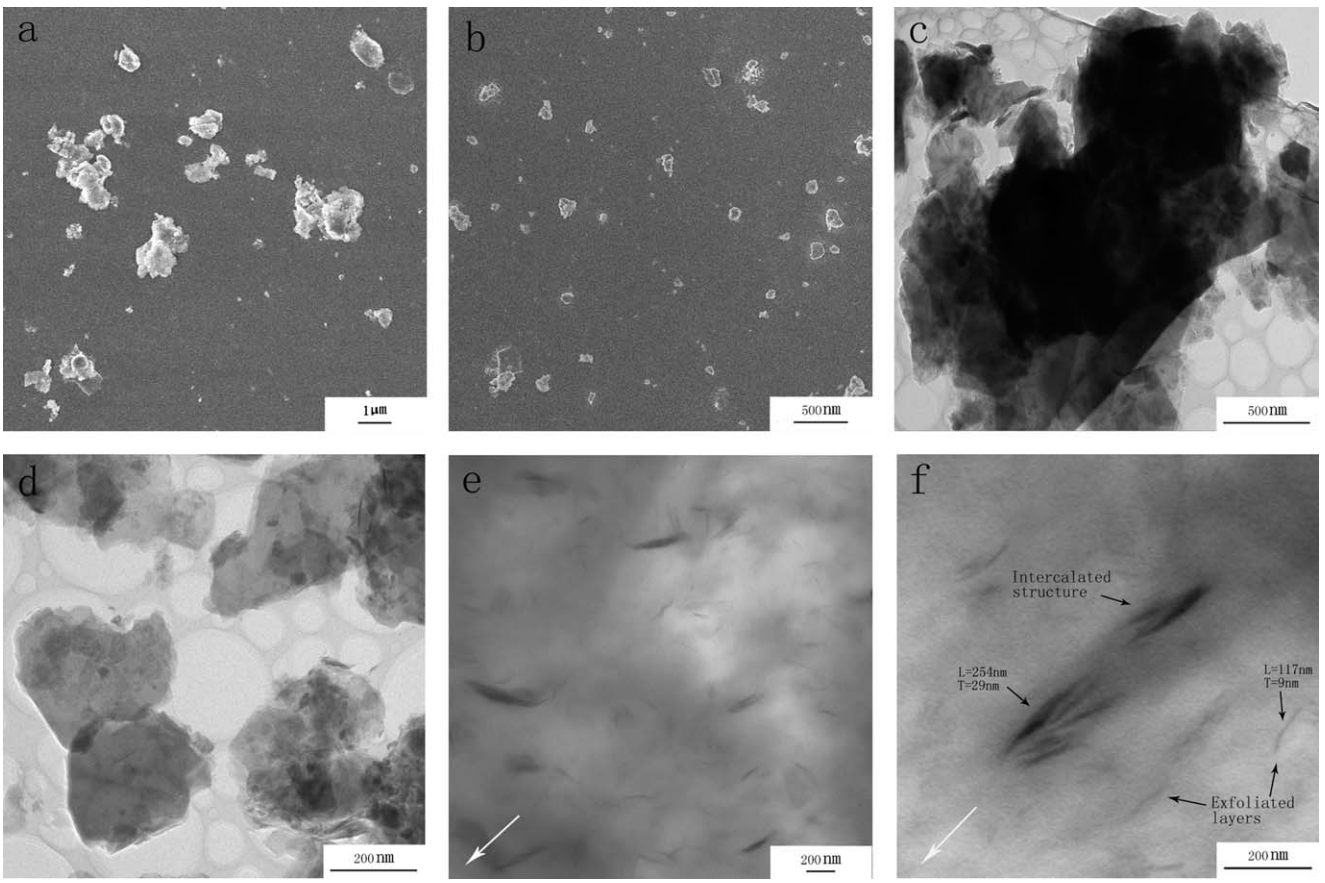

Figure 3 SEM micrographs of (a) OD and (b) ED and TEM micrographs of (c) OD, (d) ED, and (e,f) LDN-5 (the arrow is oriented parallel to the nanocomposite surface).

1464, 1708, and 3212 cm^{-1} may have been due to the formation of the decomposition products of urea, such as cyanic acid and cyanuric acid.[22]

Morphology of the dickite and LDN-5

The reduction in particle size and the associated morphological changes of dickite after the intercalation and later thermal decomposition of urea molecules were evident in the scanning electron microscopy (SEM) micrographs [Fig. 3(a,b)] and the transmission electron microscopy (TEM) micrographs [Fig. 3(c,d)]. Figure 3(a,c) shows that the OD particles, with a mean diameter of about 1 μm, were composed of thick stacking layers. As shown in Figure 3(b,d), the stacking layers were delaminated, and the particle size of the lamellar dickite decreased. No big agglomeration appeared in the SEM micrograph of ED, and the mean diameter decreased to about 200 nm. SEM and TEM examination directly displayed the exfoliation of the dickite layers and corresponded with XRD and FTIR results.

Figure 3(e,f) shows the TEM results for the LDN-5 specimen. The TEM micrographs indicated that the nanocomposite displayed a highly dispersed morphology consisting of intercalated thin tactoids with different sizes and completely exfoliated layered dickite particles of different sizes [see the arrows in Fig. 3(f)] and a small amount of nonexfoliated dickite aggregates. A combination of appropriate surface modification[26–29] and sufficiently high shear forces in the melt during polymer processing is usually required to generate extensive ratios exfoliation in nanocomposites; however, fully exfoliated systems are very seldom achieved via conventional melt-blending routes in polyolefins.[30] This nanocomposite appeared to show, however, more highly dispersed exfoliated platelets in the polyolefin matrix. Although there were clay aggregates in the microstructure of the nanocomposite, the thickness size of these in the nanometer range had a high aspect ratio.[31] The actual aspect ratio [length (L)/thickness (T)] of the individual platelets was measured to be between 10 and 20, whereas for large aggregates, an average above 5 was measured. Interestingly, as shown in Figure 3(e,f), smaller exfoliated layers appeared to be in an irregular orientation, whereas the bigger intercalated tactoids and nonexfoliated dickite aggregates were prone to parallel to the nanocomposite surface. This observation was quite

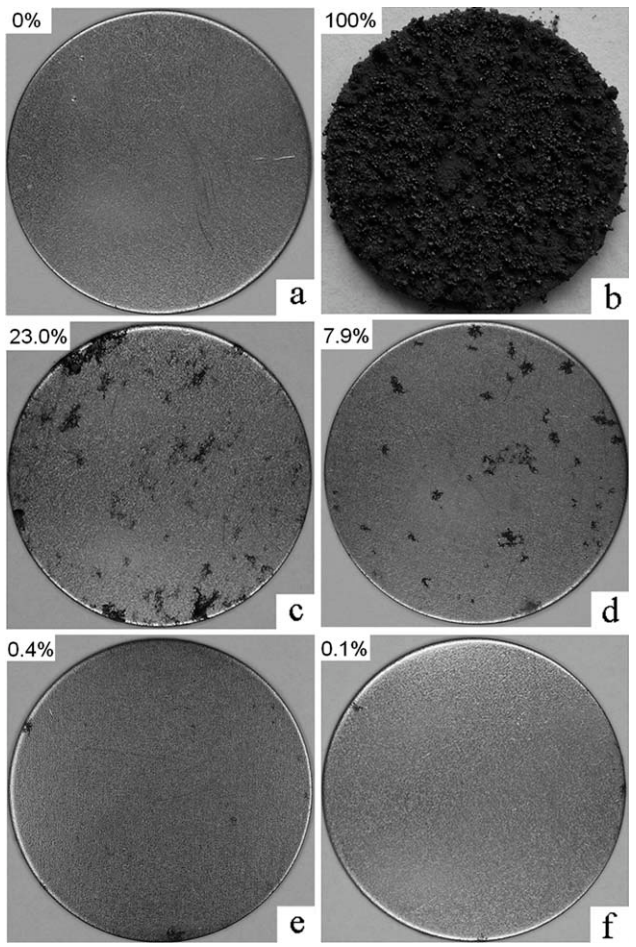

Figure 4 Photographs of the (a) original iron coupon, (b) bare iron coupon inside the testing box, and the iron coupons packed with an (c) LLDPE bag, (d) LDM-5 bag, (e) LDN-5 bag, and (f) U.S. Daubert Cromwell VCI film bag (the corrosion rate of the iron coupon is marked on each photograph).

similar to that of a LDM-5 we prepared previously.[18] Bigger layered particles in the composite may have been prone to be oriented at the process of the hot-press formation.

Performance in the salt-spray test

Figure 4 shows the photographs of the iron coupon without and with certain treatments. As the iron could not withstand the aggressive salt-spray corrosion, the bare iron coupon in the testing box was badly corroded, as shown in Figure 4(b). The corrosion degree of the iron coupon packed with the LLDPE bag decreased. However, visible rust still appeared on the surface of the iron coupon. To quantify the corrosion degree, the corrosion rate of the iron coupon was obtained by the calculation of the pixel proportion of the pitting in each photograph with Photoshop software. As shown in Figure 4(a,b), the corrosion rates of the original and bare iron coupon were 0 and 100%, respectively. The corrosion rate of the iron coupon packed with the LLDPE bag decreased to 23.0%. The anticorrosion properties of this polymer were improved because of the introduction of the dickite particles, both original ones and exfoliated ones. Compared with the iron coupon packed with the LLDPE bag, the corrosion rate of the iron coupon packed with the LDM-5 bag decreased to 7.9% [Fig. 4(d)]. As shown in Figure 4(e), only a little pitting appeared on the surface of the iron coupon packed with the LDN-5 bag; this indicated a remarkable improvement the anticorrosion properties. The corrosion protection effect of LDN-5 with a corrosion rate of 0.4% was comparable with that of the U.S. Daubert Cromwell VCI film (with a corrosion rate of 0.1%). As shown in the TEM micrographs of LDN-5 in Figure 3(e,f), parallel-oriented intercalated tactoids, nonexfoliated dickite aggregates, and highly dispersed exfoliated platelets with a high aspect ratio appeared in the microstructure of the nanocomposite. Therefore, a tortuous pathway, which retarded the progress of salt spray through the nanocomposite film, was formed. In addition, clay layer bundles strongly restricted the motion of the polymer chains; this probably decreased the coefficient of diffusion of the gas and water molecules.[32] Therefore, compared with pure LLDPE, the introduction of ED into the LLDPE matrix remarkably improved the anticorrosion properties of the polymer by impeding the penetration of the aggressive salt spray through the composite film. For LDM-5 packaging, a similar tortuous pathway was also formed;[18] this indicated improved anticorrosion properties compared with the LLDPE packaging. However, the poor dispersion of dickite particles in the LLDPE matrix shortened the tortuous pathway, and the obtained anticorrosion properties were not comparable with those of LDN-5.

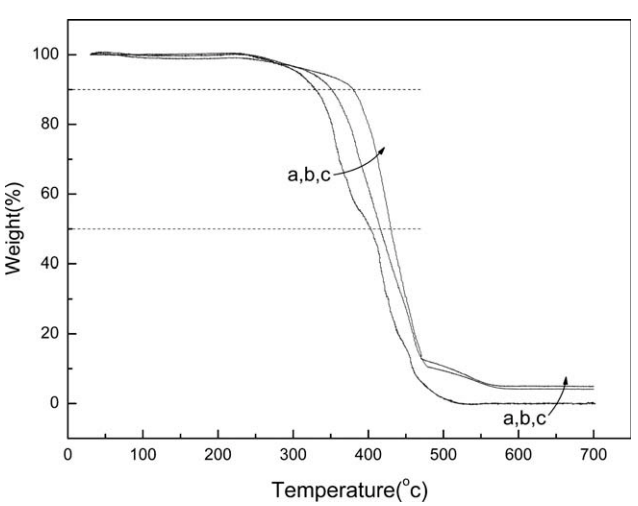

Figure 5 TG curves of (a) pure PE, (b) LDM-5, and (c) LDN-5.

TABLE II
TG Data of LLDPE, LDM-5, and LDN-5

Sample	$T_{-10\%}$ (°C)	$T_{-50\%}$ (°C)	Mass loss (250–400°C; %)
LLDPE	330	402	48.1
LDM-5	352	416	39.4
LDN-5	379	429	25.3

Thermooxidative stability of LDN-5

The TG curves of pure LLDPE, LDM-5, and LDN-5 are shown in Figure 5. In general, there were three stages of weight loss of LDM-5 and LDN-5 starting at about 50°C and ending at 700°C; these may have corresponded to the evaporation of the moisture at lower temperatures (e.g., 50–100°C), structural decomposition of the polymer backbones at higher temperatures (e.g., 230–460°C), and the dehydroxylation process of the filled dickite (e.g., 470°C).[33] Evidently, the onset of the thermooxidative decomposition of those composites shifted significantly toward the higher temperature range compared to that of pure LLDPE; this confirmed the enhancement of the thermooxidative stability of these composites.[34] After about 570°C, all of the curves became flat, and mainly, the inorganic residue (i.e., Al_2O_3, SiO_2) remained. The thermooxidative degradation temperatures corresponding to mass losses of 10 and 50% ($T_{-10\%}$ and $T_{-50\%}$, respectively) are listed in Table II. As shown in Table II, $T_{-10\%}$ and $T_{-50\%}$ increased from 330 and 402°C (pure LLDPE) to 379 and 429°C (LDN-5), respectively. At the same time, the mass loss (250–400°C) decreased from 48.1% (pure LLDPE) to 25.3% (LDN-5). The introduction of ED particles into the LLDPE matrix improved the thermooxidative stability of LDN-5. The reason may depend on the fact that the dispersed dickite platelets created a strong barrier to hinder the evaporation of small molecules generated during thermal decomposition and limited the continuous decomposition of the LLDPE matrix. Compared with LDM-5, the fully ED platelets dispersed in the LLDPE matrix at the same filler loading and formed a more tortuous pathway to hinder the diffusion and evaporation of small molecules and a thin efficient barrier to the oxygen permeation, which slowed thermooxidative degradation.[35] Therefore, LDN-5 exhibited a higher thermooxidative stability in terms of $T_{-10\%}$ and $T_{-50\%}$ than either LDM-5 or pure LLDPE.

CONCLUSIONS

We prepared ED exfoliated by the thermal decomposition of molecular urea in the interlayer of dickite. ED was composed with LLDPE to prepare the novel LDN-5. The experimental results showed that molecular urea could intercalate into the dickite interlayer by the displacement of hydrazine monohydrate molecules previously intercalated into the dickite interlayer. FTIR spectroscopy proved that hydrogen bonds were formed between the urea molecules and the inner-surface hydroxyls of dickite. The molecular urea completely expanded the dickite structure from a basal spacing of 7.22 to one of 10.68 Å. Subsequent 500°C calcination rapidly decomposed interlamellar urea molecules and produced a large amount of gases, including ammonia and carbon dioxide, which expanded the dickite interlayer and led to the exfoliation of the dickite. The weakening and broadening of the 001 XRD diffraction of dickite and the SEM and TEM micrographs effectively confirmed the thermal decomposition of the interlamellar molecular urea ED layers, which resulted in smaller particle sizes and better dispersions of dickite in the resulting LLDPE/dickite composite. Furthermore, highly dispersed clay platelets formed a more tortuous pathway, which retarded the progress of salt spray through the nanocomposite film, and therefore, the obtained anticorrosion properties of LDN-5 were better than that of the LLDPE/dickite composite. An increase in the thermooxidative stability of the nanocomposite was also observed.

References

1. Lu, H. D.; Hu, Y.; Li, M.; Chen, Z. Y.; Fan, W. C. Compos Sci Technol 2006, 66, 3035.
2. Li, P.; Tan, T. C.; Lee, J. Y. Synth Met 1997, 88, 237.
3. Barcroft, F. T.; Park, D. Wear 1986, 108, 213.
4. Chytiri, S.; Goulas, A. E.; Riganakos, K. A.; Kontominas, M. G. Radiat Phys Chem 2006, 75, 416.
5. Goulas, A. E.; Riganakos, K. A.; Kontominas, M. G. Radiat Phys Chem 2003, 68, 865.
6. Leng, A.; Stratmann, M. Corros Sci 1993, 34, 1657.
7. Lenard, D. R.; Moores, J. G. Corros Sci 1993, 34, 871.
8. Yu, Y. H.; Yeh, J. M.; Liou, S. J.; Chang, Y. P. Acta Mater 2004, 52, 475.
9. Itagaki, T.; Matsumura, A. J Mater Sci Lett 2001, 20, 1483.
10. Suh, D. J.; Lim, Y. T.; Park, O. O. Polymer 2000, 41, 8557.
11. Kotsilkova, R.; Petkova, V.; Pelovski, Y. J Therm Anal Calorim 2001, 64, 591.
12. Alexandre, M.; Dubois, P. Mater Sci Eng R 2000, 28, 1.
13. Wan, C.; Qiao, X.; Zhang, Y.; Zhang, Y. X. Polym Test 2003, 22, 453.
14. Giannelis, E. P. Adv Mater 1996, 8, 29.
15. Ding, C.; Guo, B.; He, H.; Jia, D. M.; Hong, H. Q. Eur Polym J 2005, 41, 1781.
16. Li, H.; Yu, Y. Z.; Yang, Y. K. Eur Polym J 2005, 41, 2016.
17. Michalkova, A.; Tunega, D.; Nagy, L. T. J Mol Struc-Theochem 2002, 581, 37.
18. Xue, B.; Jiang, Y. S.; Li, F. F.; Xia, M. S.; Sun, M. M.; Liu, D. R.; Zhang, X. G.; Yu, L. X. J Appl Polym Sci 2010, 116, 3480.
19. Rutkai, G.; Makó, É.; Kristóf, T. J Colloid Interface Sci 2009, 334, 65.
20. Valášková, M.; Rieder, M.; Matějka, V.; Čapková, P.; Slíva, A. Appl Clay Sci 2007, 35, 108.
21. Onoda, H.; Nariai, H.; Maki, H.; Motooka, I. J Mater Synth Process 2002, 10, 121.

22. Abramova, E.; Lapides, I.; Yariv, S. J Therm Anal Calorim 2007, 90, 99.
23. Madejová, J. Vib Spectrosc 2003, 31, 1.
24. Ledoux, R. L.; White, J. L. Silic Ind 1967, 32, 269.
25. Frost, R. L.; Tran, T. H. T.; Kristóf, J. Clay Miner 1997, 32, 587.
26. Akbulut, S.; Arasan, S.; Kalkan, E. Appl Clay Sci 2007, 38, 23.
27. Argun, M. E.; Dursun, S. Bioresour Technol 2008, 99, 2516.
28. Kornilov, V. M.; Lachinov, A. N. Microelectron Eng 2003, 69, 399.
29. Lemić, J.; Tomašević-Čanović, M.; Djuričić, M.; Stanić, T. J Colloid Interface Sci 2005, 292, 11.
30. Sanchez-Garcia, M. D.; Gimenez, E.; Lagaron, J. M. J Appl Polym Sci 2008, 108, 2787.
31. Park, J. H.; Jana, S. C. Polymer 2003, 44, 2091.
32. Yariv, S. Appl Clay Sci 2004, 24, 225.
33. Franco, F.; Cruz, M. D. R. J Therm Anal Calorim 2006, 85, 369.
34. Yeh, J. M.; Kuo, T. H.; Huang, H. J.; Chang, K. C.; Chang, M. Y.; Yang, J. C. Eur Polym J 2007, 43, 1624.
35. Ravadits, I.; Tóth, A.; Marosi, G.; Márton, A.; Szép, A. Polym Degrad Stab 2001, 74, 419.